

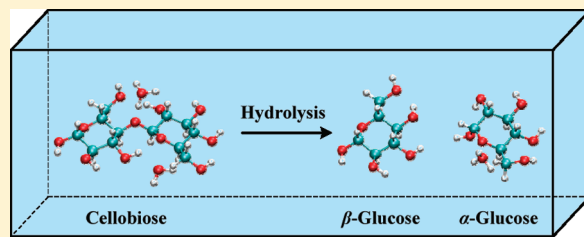
Local Site Selectivity and Conformational Structures in the Glycosidic Bond Scission of Cellobiose

Xiao Liang, Alejandro Montoya,* and Brian S. Haynes

School of Chemical and Biomolecular Engineering, The University of Sydney, Sydney, NSW 2006, Australia

 Supporting Information

ABSTRACT: Car–Parrinello molecular dynamics combined with metadynamics simulations were used to study the acid-catalyzed hydrolysis of cellobiose (CB) in aqueous solution. The hydrolysis was studied in two steps. Step 1 involves the proton transfer from solvent to CB and dissociation of the glycosidic bond to β -glucose and oxacarbenium ion species. Step 2 involves the formation of α -glucose from oxacarbenium and regeneration of the acid proton species. Step 1 is endothermic, while Step 2 is exothermic. The overall activation free energy of CB hydrolysis is 32.5 kcal mol⁻¹, and the overall reaction free energy is -5.9 kcal mol⁻¹, consistent with available experimental data. We observe that a stepwise mechanism generally described in the literature for Step 1 is not significantly favored relative to a concerted β -1,4' linkage dissociation process.



1. INTRODUCTION

Hydrolysis of polysaccharides and oligosaccharides is attracting a rapidly increasing interest because these compounds contain functionalities similar to those in hemicelluloses. Cellobiose (CB) is a disaccharide that contains two glucose units bound by a glycosidic β -1,4' linkage and constitutes the repeating disaccharide unit of cellulose. Elucidation of the scission mechanism of the β -1,4' linkage of CB is of fundamental importance to the understanding of the dynamics of cellulose chain hydrolysis during biomass degradation processes.

In water under ambient conditions, hydrolysis of CB is inefficient, giving a low rate of product formation. Acids catalyze the hydrolysis process.¹ Degradation of CB at low temperatures (80–150 °C) under dilute acid conditions proceeds via hydrolysis of the glycosidic bond to produce glucose following pseudofirst-order kinetics with an activation energy that ranges from 30 to 35 kcal mol⁻¹.^{1,2} The glucose condensation to produce multiple disaccharides, including CB in mildly acidic solution in the temperature range 100–170 °C follows second-order kinetics with the energy barriers falling in the range of 28–34 kcal mol⁻¹.³ Condensation reactions appear to occur mainly through the anomeric carbon atom (C1) of one glucose residue linking with disparate hydroxyl or hydroxymethyl groups of the second glucose molecule.³ The enthalpy of hydrolysis of CB to α -glucose at 298 K is reported to be -0.6 kcal mol⁻¹ based on calorimetric measurements, and in the range of -4.3 to -5.3 kcal mol⁻¹ based on enthalpies of solution and combustion,^{4,5} providing a measure of the uncertainties in the available thermodynamic information.

It is generally accepted that hydrolysis of CB follows the mechanism of polysaccharide and oligosaccharide hydrolysis. The acid-catalyzed process is postulated to follow a stepwise reaction mechanism controlled by the formation

of an oxacarbenium species.^{6,7} Initially, CB and the acid proton (H_3O^+) interact and establish equilibrium with an oxonium species ($>\text{C}-\text{OH}-\text{C}<$). The oxonium subsequently decomposes into glucose ($>\text{C}-\text{OH}$) and oxacarbenium ion ($>\text{C}^+$). The oxacarbenium ion is solvated to produce glucose and regenerate the acid proton. Formation of the oxonium and oxacarbenium ions is, however, a matter of debate given the extremely short-lived existence of these species,⁸ and inconclusive experimental evidence exists to determine whether the hydrolysis follows a cyclic or open oxacarbenium species.⁹

A constrained Car–Parrinello molecular dynamics (CPMD) study of the acid-catalyzed condensation of glucose with methanol indicated that the oxacarbenium intermediate has insufficient time to reach equilibrium with the solvent (nonsolvent equilibrated) before the subsequent substitution reaction takes place, and the hydrogen bond and aqueous solvent therefore play an active role in the reaction.¹⁰ Molecular dynamics combined with metadynamics studies carried out on the dehydration of pyranoses (glucose and xylose) and scission of the β -1,4' linkage of xylobiose support the formation of oxonium and oxacarbenium species.^{11,12} These studies revealed an important dynamic effect of explicit water molecules in the protonation/deprotonation reactions of saccharides. The reactions in solution are solvent-induced due to the proton's high affinity for water molecules, indicating that solvent reorganization should be considered in order to determine Gibbs free energies and structural conformations.^{11,12} A QM/MM study on the acid-catalyzed conversion of fructofuranose into 5-hydroxymethyl furfural revealed that the first dehydration step generates a stable oxacarbenium

Received: May 6, 2011

Revised: July 29, 2011

Published: July 29, 2011

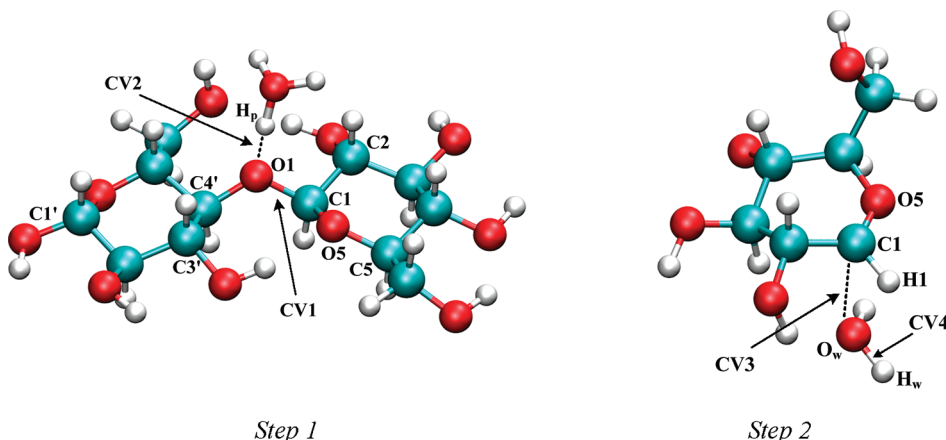


Figure 1. Selected CVs in the acid-catalyzed hydrolysis of *syn*-CB. Step 1: scission of O1–C1 glycosidic bond (CV1) and protonation of glycosidic oxygen O1 (CV2). Step 2: formation of α -glucose (CV3) and regeneration of acid proton (CV4).

ion species via the protonation of the hydroxyl group on the anomeric carbon, and that the reorganization of solvent has a significant effect on reducing the corresponding energy barrier.¹³

Computational modeling of CB hydrolysis to glucose has been constrained by the presence of a considerable number of energetically degenerate conformational structures. Separate detailed analyses of the conformers of CB,¹⁴ CB–water intermediates,¹⁵ and glucose^{16–20} have now been reported. Vibrational spectroscopy under molecular beam conditions²¹ and density functional theory (DFT) studies^{14,15} show that CB and monohydrated CB slightly favor the CB *anti*-configurations in gas phase. In contrast to this, the CB units of cellulose chains,^{22–24} crystalline CB,^{25,26} and CB in aqueous phase^{27,28} adopt linear *syn*-conformations. The data obtained from molecular dynamics calculations indicated that the *syn*- to *anti*- ratio in solution is 93:7 at 300 K.²⁹ In this study, we applied *ab initio* DFT molecular dynamics to study the acid-catalyzed hydrolysis of CB in order to obtain a robust statistical treatment of the system. We used a *syn*- initial configuration of CB, and the conformational changes of CB are monitored as the hydrolysis reaction proceeds. Since the rate of hydrolysis is slow and exceedingly lengthy molecular dynamics computations would be required, we have used the Car–Parrinello metadynamics technique³⁰ to explore the reaction mechanism and access the corresponding free energy landscape in a reasonable computational time. In the metadynamics approach, a repulsive biasing potential is established where the system would otherwise spend most of its time, thereby allowing the system to escape local energy minima and cross energy barriers.³¹ The metadynamics approach has successfully been applied to a number of reaction systems and has been proved to provide accurate thermodynamic information for liquid-phase reaction systems.^{32–34} This paper explores the local site selectivity during protonation and dissociation of the glycosidic β -1,4' linkage, the conformational structures along the hydrolysis reaction coordinate, and the free energy of reaction.

2. COMPUTATIONAL METHODOLOGY

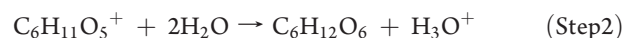
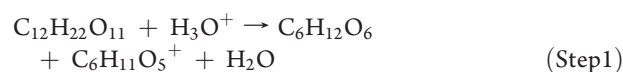
Density functional CPMD simulations were carried out in this study using the CPMD program.³⁵ Goedecker pseudopotentials³⁶ were used to describe the inner electronic shells of ions, and the Becke, Lee, Yang, and Parr (BLYP) functional was used to describe the valence electrons.^{37,38} A plane wave cutoff of 70

Ry was used for the Kohn–Sham orbitals. The equations of motion were integrated with a time step of 4 au (0.1 fs) and a fictitious mass of 800 amu for electrons was used.

The CPMD simulations were conducted under the NVT ensemble at 300 K with a Nose–Hoover chain thermostat.³⁹ A periodic supercell with dimensions of 22.5 Å × 13.0 Å × 10.0 Å was used. The unit cell contains 69 water molecules, 1 CB molecule, 1 hydronium ion (H_3O^+), and 1 chloride ion (Cl^-). The chloride ion acting as a counterion was used to maintain electric neutrality of the system. During the simulations, the chloride anion is observed to always stay in the second solvation shell of CB without interacting with H_3O^+ or participating in the reaction. The involvement of a chloride counterion to neutralize the simulated system has been used in several studies of acid-catalyzed reactions.^{11,12,40} The corresponding density of solution is 930.5 g L⁻¹, and the concentrations of CB and H_3O^+ are both 0.57 mol L⁻¹.

The initial configuration was obtained by inserting one optimized isolated *syn*-CB molecule, one hydrogen, and one chloride atom into a box containing solvent molecules in equilibrium, and deleting the water molecules that are overlapped by the CB molecule. The isolated *syn*-CB molecule was optimized using the Gaussian 09 package⁴¹ at the B3LYP/6-31G(d,p) level, while the equilibrium configuration of solvent molecules was achieved from a Monte Carlo simulation using the DICE program.⁴² A four-picosecond CPMD calculation was then conducted on the created supercell to equilibrate the system before performing the metadynamics simulations.

We studied the acid-catalyzed hydrolysis of CB in two steps. Step 1 involves the proton transfer from solvent to the glycosidic oxygen and the subsequent dissociation of the glycosidic bond to form β -glucose and one oxacarbenium ion species. Step 2 involves the formation of a second glucose molecule and regeneration of the acid proton species:



Potential free energy surfaces for Step 1 and Step 2 were generated from metadynamics simulations⁴³ by biasing the dynamics with a history-dependent potential. This biasing

Table 1. Control Parameters of the Selected CVs during Our CPMD Metadynamics Computations

	$d_0(\text{\AA})$	m (amu)	k (au)
CV1	2.0	600	8.0
CV2	1.5	100	3.0
CV3	2.0	600	8.0
CV4	1.5	100	3.0

potential can act as a coarse-grained representation of the system providing free energies that depend on a set of predefined collective variables (CVs) that characterize the reaction coordinate. In this study, two CVs were selected for each step as presented in Figure 1. CV1 is defined as the coordination number (CN) changes of C1 with respect to the glycosidic oxygen atom O1, while CV2 represents the CN changes of proton H_P with respect to O1. The symbol H_P is used to represent the closest hydrogen atom to O1. CV1 describes the dissociation of the glycosidic bond, and CV2 describes the proton transfer from solvent to CB. In Step 2, CV3 corresponds to the CN changes of C1 with respect to O_W, and CV4 corresponds to CN changes of H_W with respect to O_W. CV3 describes the nucleophilic attack of H₂O, and CV4 describes the proton regeneration.

In all cases, the CN values are defined by the following equation:⁴⁴

$$\text{CN} = \frac{1 - (d_{ij}/d_0)^p}{1 - (d_{ij}/d_0)^p + q} \quad (\text{E.1})$$

where d_{ij} is the distance between atoms i and j , d_0 is the reference distance, and $p = q = 6$ are constants to distinguish between the coordinated and noncoordinated states. The CN value between two atoms indicates whether a covalent bond exists ($1 = \text{bond}$, $0 = \text{no bond}$). The selected values of cutoff distance d_0 for all selected CVs are shown in Table 1 coupled with the parameters of fictitious masses (m) and force constants (k), which control the dynamics of the fictitious CVs.

A normal Gaussian bias potential was employed in the metadynamics simulations. The width of Gaussian potential was set to 0.05 au in all simulations. The heights of the Gaussian hills in the proton transfer and dissociation of the glycosidic bond of CB were determined by the shape of the underlying energy surface and set to be at most 3.8 kcal mol⁻¹. The average hill height in the simulation of Step 1 was 1.9 kcal mol⁻¹. The heights of the Gaussian hills in the proton regeneration were set at 0.3 kcal mol⁻¹. The addition of bias potential was allowed with a minimum time separation of 100 molecular dynamics steps and with the displacements in CVs being larger than 1.5 times the width of Gaussian function. The addition of consecutive potentials was forced after 300 molecular dynamics steps if the displacement had not exceed the threshold. Similar settings in previous studies were shown to enable accurate prediction of the energetics and dynamics of hydrolysis of esters and sugars in aqueous solution.^{45–47} The molecular graphics were rendered with VMD.⁴⁸

Inside our unit cell, CB is surrounded by two water shells, which hinders the CB interaction with the CB molecules located in adjacent periodic unit cells. Due to the finite size of our unit cell, the metadynamics free energy maps inevitably contain the CB–proton interaction in the reactant energy basin and

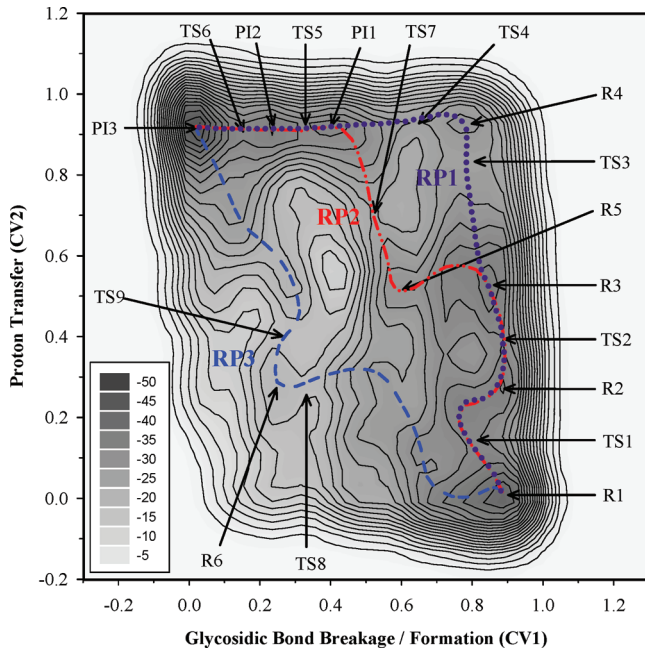


Figure 2. Two-dimensional free energy landscape of the reaction $\text{C}_{12}\text{H}_{22}\text{O}_{11} + \text{H}_3\text{O}^+ \rightarrow \text{C}_6\text{H}_{12}\text{O}_6 + \text{C}_6\text{H}_{11}\text{O}_5^+ + \text{H}_2\text{O}$ in aqueous phase at 300K (energy in kcal mol⁻¹). The pathways RP1 (R1 → TS4 → PI3), RP2 (R1 → TS7 → PI3), and RP3 (R1 → TS9 → PI3) are shown as purple dotted, red dashed-dotted, and blue dashed lines, respectively. The energy scale is given in the inset to the left; contour lines in the figure are spaced 2.0 kcal mol⁻¹ apart. Positions R, TS, and PI in the energy landscape correspond to selected key conformations of the reactant, transition state, and product basins, respectively, which are presented in Figure 3.

glucose–glucose interaction with the proton species in the product energy basin. We have estimated the required energy for infinite separation of the reactants and products by performing static electronic calculations on the reactants and products. Static calculations were carried out in Gaussian 09⁴¹ for optimizing the electronic structures and estimating the solvation free energies of reactant complexes. The geometry optimizations were computed at the B3LYP/6-31G(d,p) level of theory. The nature of the structures in equilibrium was determined by performing a normal-mode analysis. The minima are characterized by possessing all real vibrational frequencies and a Hessian matrix with all eigenvalues positive. The unscaled frequencies were used to obtain corrections for Gibbs free energies. Previous DFT studies have shown that intramolecular hydrogen bond interactions require diffuse functions in the basis sets in order for the relative stability of monosaccharides to be predicted accurately.^{49–51} In this study, the electronic energy was computed using the 6-311++G(d,p) basis set on the equilibrium structures obtained using the 6-31G(d,p) basis set, B3LYP/6-311++G(d,p)//B3LYP/6-31G(d,p).

The Gibbs free energy in solution with a 1 molar (1M) standard-state basis was calculated using the change in Gibbs free energy in the gas phase, $\Delta G_{g,1M}$, corrected by the differential Gibbs free energy of solvation ($\Delta\Delta_s G$). The $\Delta\Delta_s G$ was calculated as the difference in free energy of solvation, $\Delta_s G$:

$$\begin{aligned} \Delta G_{aq} &= \Delta G_{g,1M} + \Delta\Delta_s G \\ &= \Delta G_{g,1M} + \sum (\Delta_s G)_{\text{prod}} - \sum (\Delta_s G)_{\text{react}} \end{aligned} \quad (\text{E.2})$$

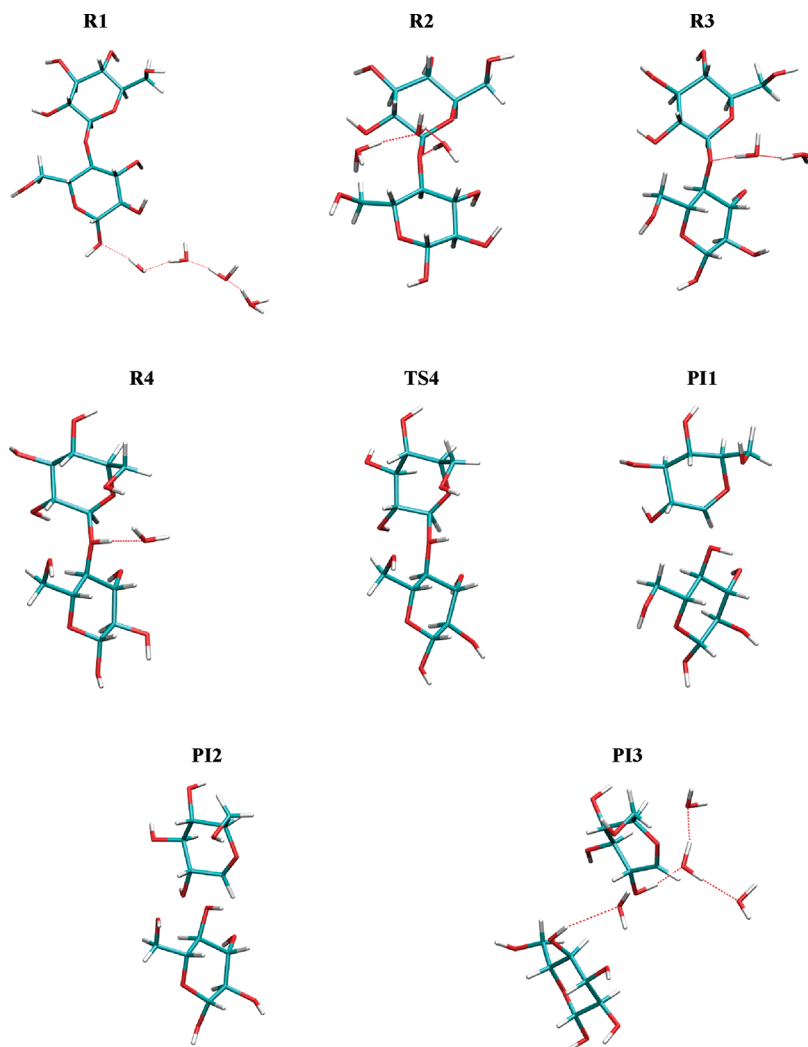


Figure 3. Snapshots from metadynamics simulations of the reaction $\text{C}_{12}\text{H}_{22}\text{O}_{11} + \text{H}_3\text{O}^+ \rightarrow \text{C}_6\text{H}_{12}\text{O}_6 + \text{C}_6\text{H}_{11}\text{O}_5^+ + \text{H}_2\text{O}$ along the energy minimal reaction pathway RP1.

Gibbs free energies of solvation in water solution ($\Delta_s G$) were calculated by means of the SMD model.⁵² We have determined the $\Delta_s G$ of all species using the B3LYP/6-311++G(d,p) basis set on the equilibrium configurations in the gas phase. The molar Gibbs free energy in gas phase, $\Delta G_{g,1M}$, is calculated from the Gibbs free energy in the gas-phase at 1 atm standard-state, $\Delta G_{g,1atm}$, and the ratio of concentrations (Q) as appearing in the equilibrium constant evaluated with all species at their standard-state concentration:⁵³

$$\Delta G_{g,1M} = \Delta G_{g,1atm} + RT \ln(Q_{1M}/Q_{1atm}) \quad (\text{E.3})$$

where R is the gas constant and T is temperature. $\Delta G_{g,1atm}$ is calculated using the enthalpy ($\Delta H_{r,1atm}$) and entropy changes ($\Delta S_{r,1atm}$). The enthalpy and entropy changes are computed using the optimized gas-phase species and are calculated by including the effects of vibration, translation, and rotation.

3. RESULTS AND DISCUSSIONS

3.1. Protonation and Dissociation of Glycosidic β -1'

Linkage. Figure 2 presents the free energy surface as a function of CV1 (β -1,4' glycosidic bond scission) and CV2 (proton

transfer from solvent to the glycosidic oxygen). Figures 3 and 4 present selected snapshots collected from the metadynamics simulations corresponding to the energy surface in Figure 2. For clarity of presentation, the redundant solvent molecules of every configuration in Figures 3 and 4 are deleted. The complete configurations of each snapshot including all the water molecules used in our simulations are presented in Figures SI1 and SI2 of the Supporting Information

The average bond lengths and their corresponding standard deviations in every energy basin are presented for selected bonds in Table 2. The standard deviations are computed from the configurations falling within ~ 1.5 kcal mol⁻¹ of each energy minimum.

The bottom of the energy landscape in Figure 2 is found at R1, located at CV1 = 0.89 and CV2 = 0.01. The configuration of R1 corresponds to CB solvated in water. Here, the proton is in favor of forming a H_5O_2^+ species in the second solvation shell, indicating a higher proton affinity toward water molecules than toward CB. The acid proton interacts with the $-\text{OH}$ group on C1' via four hydrogen bonds (as shown in R1 in Figure 3). The average bond lengths of the glycosidic group are C1'-O1 = 1.45 Å, and C4'-O1 = 1.48 Å. The glycosidic group is therefore

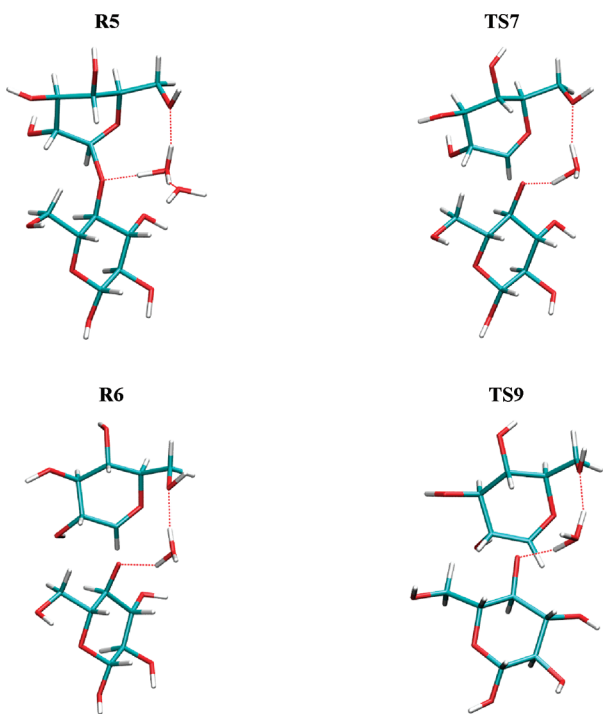


Figure 4. Snapshots from metadynamics simulations of the reaction $\text{C}_{12}\text{H}_{22}\text{O}_{11} + \text{H}_3\text{O}^+ \rightarrow \text{C}_6\text{H}_{12}\text{O}_6 + \text{C}_6\text{H}_{11}\text{O}_5^+ + \text{H}_2\text{O}$ along the reaction pathways RP2 and RP3.

Table 2. Average Bond Lengths and Corresponding Standard Deviations (in Å) of Selected Configurations along the Reaction Pathway $\text{C}_{12}\text{H}_{22}\text{O}_{11} + \text{H}_3\text{O}^+ \rightarrow \text{C}_6\text{H}_{12}\text{O}_6 + \text{C}_6\text{H}_{11}\text{O}_5^+ + \text{H}_2\text{O}^a$

	C1–O1	H _p –O1	C1–O _W	C4'–O1	C1–O5
R1	1.45 ± 0.06	3.25 ± 0.07	5.05 ± 0.45	1.48 ± 0.04	1.45 ± 0.04
R2	1.43 ± 0.03	1.75 ± 0.03	4.68 ± 0.61	1.47 ± 0.03	1.46 ± 0.03
R3	1.54 ± 0.04	1.47 ± 0.04	4.36 ± 0.87	1.48 ± 0.02	1.43 ± 0.05
R4	1.64 ± 0.03	0.97 ± 0.02	4.16 ± 0.40	1.55 ± 0.06	1.39 ± 0.03
TS4	1.85 ± 0.06	1.00 ± 0.03	4.15 ± 0.27	1.53 ± 0.06	1.34 ± 0.03
PI1	2.13 ± 0.06	1.00 ± 0.03	4.37 ± 0.39	1.50 ± 0.03	1.30 ± 0.03
PI2	2.41 ± 0.05	1.03 ± 0.03	4.39 ± 0.55	1.51 ± 0.04	1.29 ± 0.03
PI3	5.04 ± 0.72	0.98 ± 0.05	2.70 ± 0.36	1.49 ± 0.05	1.29 ± 0.02
R5	1.85 ± 0.04	1.49 ± 0.02	4.13 ± 0.77	1.47 ± 0.03	1.35 ± 0.05
TS7	1.99 ± 0.04	1.30 ± 0.04	3.44 ± 0.24	1.48 ± 0.02	1.31 ± 0.03
R6	2.70 ± 0.94	1.75 ± 0.18	3.63 ± 0.49	1.44 ± 0.06	1.31 ± 0.02
TS9	2.38 ± 0.02	1.59 ± 0.02	3.88 ± 0.74	1.48 ± 0.06	1.31 ± 0.03

^a Atom nomenclature is presented in Figure 1.

geometrically unsymmetrical. The C1–O1 and C4'–O1 bond lengths in cellulose are 1.43 and 1.44 Å, respectively.²⁴ In crystalline CB, the C1–O1 and C4'–O1 bond lengths are 1.37 and 1.47 Å, respectively.²⁵

Inspection of the free energy surface shows three distinct reaction pathways of acid-catalyzed dissociation of CB, indicated by the dotted lines in Figure 2. The three different reaction pathways are in the directions of R1→TS4→PI3 (denoted RP1), R1→TS7→PI3 (RP2), and R1→TS9→PI3 (RP3), with corresponding local energy barriers of 15.8, 17.6, and 25.0 kcal mol⁻¹ with respect to the free energy of R1.

RP1 (R1→TS4→PI3) proceeds via interaction of the glycosidic oxygen with solvent and acid proton. The proton is observed to be transferred toward O1 via adjacent water molecules. This leads to the formation of two reactant intermediates, R2 (CV1 = 0.89 and CV2 = 0.28) and R3 (CV1 = 0.86 and CV2 = 0.52), which are located at 6.4 kcal mol⁻¹ and 5.5 kcal mol⁻¹ above the energy basin R1, respectively. The corresponding energy barriers R1→TS1 and R1→TS2 are 8.8 kcal mol⁻¹ and 9.0 kcal mol⁻¹, respectively. The average distance H_p···O1 in R2 is 1.75 Å, indicating that a hydrogen bond has been established between O1 and a solvent molecule. In R2, the acid proton is positioned in the first solvation shell and interacts with the glycosidic oxygen via three hydrogen bonds. The average bond length C1–O1 in R2 is 1.43 Å, very close to the length of this bond in R1. State R2 represents a reactant intermediate where the acid proton is in the first water layer of CB, and the energy barrier at TS1 corresponds to the proton transfer from the second to the first solvation shell. Inspection of R3 configuration in Figure 3 shows that the proton has moved to the side of CB, and the number of hydrogen bonds between the proton and O1 has decreased to 2. The average distance H_p···O1 in R3 further decreases to 1.47 Å, while the average bond length C1–O1 increases to 1.54 Å. The reducing glucosyl ring of CB along the C1–O1 bond is slightly rotated. This change reduces the steric hindrance of proton attack that the –OH group at C3' normally provides. The snapshot of R3 clearly indicates that O1 interacts straightforwardly with a H₅O₂⁺ species, which is ready to attack the glycosidic bond and trigger its dissociation. The energy barrier at TS2 corresponds to the process of proton transfer from the first solvation shell of CB to the vicinity of the glycosidic oxygen.

The hydrolysis along the RP1 continues as CV2 increases, forming protonated CB as observed in Figure 3, intermediate R4. Here, CV1 is 0.78 and CV2 is 0.93. The free energy of R4 is 12.1 kcal mol⁻¹ above R1. The transition state TS3 connecting R3 and R4 is at CV1 = 0.75 and CV2 = 0.84, and the corresponding energy barrier of the proton transfer to O1 is 15.4 kcal mol⁻¹ with respect to the energy of R1. Inspection of R4 configuration in Figure 3 indicates that the distance H_p···O1 decreases to 0.97 Å, suggesting that the proton has been completely transferred. The C1–O1 bond length increases to 1.64 Å, 13.1% elongated from the average value in R1; at the same time, the C1–O5 bond length has decreased to 1.39 Å, 0.06 Å shorter than in R1. The coupling of the elongation of C1–O1 with the shortening of the C1–O5 bond is consistent with the observations in glucose and methanol condensation reaction.¹⁰ This stretch of glycosidic bond consequently enhances the substantial positive charge on the anomeric C1 atom. As a result, the configuration of the nonreducing glucosyl ring starts to change from the initial ⁴C₁ configuration to a conformation close to E₃, and a slight movement of the –CH₂OH group on C5 from an equatorial position toward the top of the nonreducing glucosyl ring occurs during the reorganization of the ring conformation. The conformational changes are consistent with previous indications that β-configured glucopyranosyl donors exhibited abrupt conformational changes during the ionization reaction when the glycosidic bond length reaches a value 12–15% greater than its equilibrium value, with the resulting conformation depending strongly on the leaving group.⁵⁴ The modification of the nonreducing glucosyl ring also agrees with the principles of stereoelectronic theory, which dictates that a delocalization of nonbonded electrons of heteroatom O5 into the anomeric carbon atom C1 forces the C5, O5, C1, and C2 atoms of the glucopyranose ring to be

coplanar, thereby assisting to stabilize the electron-deficient glucosyl residue.^{55,56}

Dissociation of protonated CB occurs between the potential wells R4 and PI1 (Figure 2). The maximum value of the free energy along the reaction pathway RP1 appears at the point where $CV_1 = 0.65$ and $CV_2 = 0.93$, corresponding to TS4. The transition state TS4 is 15.8 kcal mol⁻¹ above R1. The snapshot of TS4 in Figure 3 shows a nascent β -glucose and an oxacarbenium ion species. The glycosidic bond C1–O1 has been stretched to 1.85 Å, which is 0.40 Å (27.8%) longer than the average bond length in R1. The C1–O5 bond length at TS4 is 1.34 Å, which is 0.11 Å shorter than the C1–O5 bond in R1, indicating that a lone electron pair at ring oxygen O5 has participated in the reaction by forming a partial double bond with C1, again consistent with the principles of stereoelectronic chemistry mentioned above. The –CH₂OH group on C5 is observed to move further toward the perpendicular position above the glucosyl ring.

Further separation of the oxacarbenium species from β -glucose leads to the formation of a product intermediate PI1 ($CV_1 = 0.40$ and $CV_2 = 0.92$), and further to the formation of PI2 ($CV_1 = 0.23$ and $CV_2 = 0.91$) and PI3 ($CV_1 = 0.01$ and $CV_2 = 0.92$). The system gains 21.0 kcal mol⁻¹ after passing TS4 to reach PI3. The energy barriers connecting PI1 with PI2 and PI2 with PI3 are 0.7 and 2.5 kcal mol⁻¹. The glycosidic C1–O1 bond lengths at PI1, PI2, and PI3 are 2.13, 2.40, and 5.04 Å, respectively, while the corresponding bond lengths of C1–O5 are 1.30, 1.29, and 1.29 Å, respectively. The calculated lengths of the partial double bond C1–O5 in PI2 and PI3 agree well with the value obtained from the simulations on cellulose hydrolysis catalyzed by enzymes.⁴⁶ The ring form of the oxacarbenium species is observed to change completely to a ⁴H₃ half-chair conformation in PI2. Therefore, the free energy difference between PI1 and PI2 is associated with the process of oxacarbenium ion detachment from the generated β -glucose and a slow conformational transformation of oxacarbenium ion from an envelope to a half-chair form.

Inspection of the configuration of state PI3 in Figure 3 shows that several water molecules have diffused to the area between β -glucose and oxacarbenium ion, indicating that these two species have been separated in different solvation shells. In particular, one water molecule is positioned between glycosidic oxygen O1 and anomeric C1, interacting with C1 at an average distance of 3.34 Å, and accepting a weak hydrogen bond from –H_PO1. At the same time, the nucleophilic water molecule is observed to adsorb on the anomeric C1 from the other side of the oxacarbenium ion; i.e., the distance between C1 and O_W is 2.70 Å. These observations suggest that the oxacarbenium ion is solvent-equilibrated during the CB dissociation process.

The second-lowest energy pathway (RP2) follows the potential wells R1→TS7→PI3, highlighted with the dash red line in Figure 2. The free energy barrier of this hydrolysis pathway is 1.8 kcal mol⁻¹ higher than that of RP1. The reaction pathway RP1, as discussed above, represents a stepwise hydrolysis process in which the glycosidic oxygen is protonated, followed by dissociation of the glycosidic bond. Instead, the reaction pathway RP2 represents a concerted hydrolysis process in which the protonation of the glycosidic oxygen and scission of the glycosidic bond occur simultaneously.

The concerted reaction pathway is promoted by the formation of a potential well R5, located at $CV_1 = 0.59$ and $CV_2 = 0.51$ (Figure 2). The bottom of R5 is 11.6 kcal mol⁻¹ above R1. The snapshot of R5 in Figure 4 indicates that the proton has

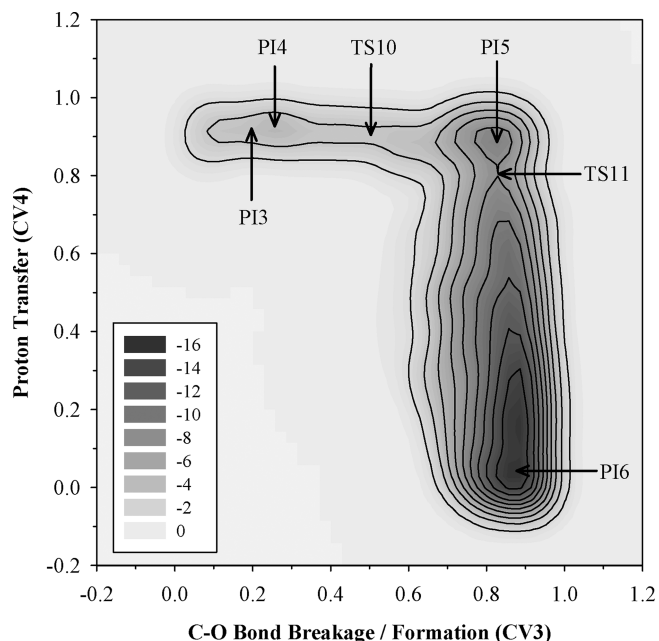


Figure 5. Two-dimensional free energy landscape of the reaction $C_6H_{11}O_5^+ + 2H_2O \rightarrow C_6H_{12}O_6 + H_3O^+$ in aqueous phase at 300 K (energy in kcal mol⁻¹). The energy scale is given in the inset to the left; contour lines in the figure are spaced 1.5 kcal mol⁻¹ apart. Positions TS and PI in the energy landscape correspond to selected key conformations of the transition state and product basins, which are presented in Figure 6.

transferred to the side of CB and interacts with the glycosidic oxygen O1 at a distance of 1.49 Å. The C1–O1 and C1–O5 bond lengths are 1.85 and 1.35 Å. The configuration of the nonreducing glucosyl ring of CB at R5 changes to a ⁴E conformation. Dissociation of C1–O1 in the concerted process occurs at TS7, which is located at $CV_1 = 0.52$ and $CV_2 = 0.70$. The energy difference between TS7 and R1 is 17.6 kcal mol⁻¹, corresponding to the highest overall energy barrier along RP2. The average bond lengths H_P–O1, C1–O1 and C1–O5 are 1.30, 1.99, and 1.31 Å, respectively, indicating that the transfer of proton to O1, the dissociation of glycosidic bond, and the formation of the partial double bond between C1 and O5 are concerted. The reaction reaches the product intermediate PI1 after passing TS7 and then follows the same reaction pathway as RP1.

A third energy pathway, RP3 (R1→TS9→PI3) is highlighted with a blue dashed line in Figure 2. RP3 represents the rupture of the glycosidic bond before the proton is transferred to O1. The free energy barrier of this hydrolysis pathway is 9.2 kcal mol⁻¹ higher than that of RP1. This energy pathway is energetically unfavored with respect to the concerted and the stepwise hydrolysis processes, possibly because the thermal cleavage of the glycosidic bond generates two charged residues that are electronically unstable. The snapshot of R6 in Figure 4 shows that the proton is located at a distance H_P–O1 of 1.75 Å. The average bond lengths of C1–O1 and C1–O5 at R6 are 2.70 Å and 1.31 Å, respectively. This indicates that the glycosidic bond has already been broken and the partial double bond of C1–O5 has almost been established, which can be also confirmed by the clear ⁴H₃ half-chair conformation of the generated oxacarbenium species. Therefore, the process from R1 to R6 can be interpreted as the thermal cleavage of the glycosidic bond, coupled with the

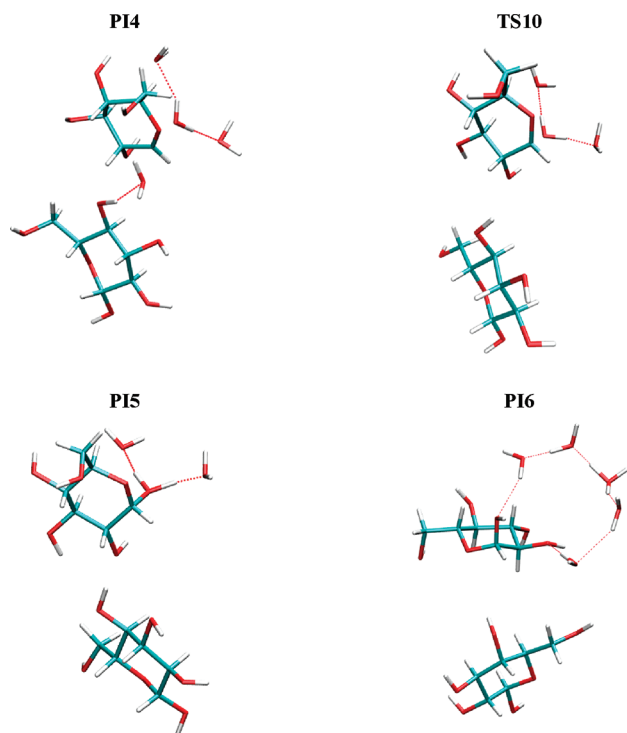


Figure 6. Snapshots from metadynamics simulations of the reaction $\text{C}_6\text{H}_{11}\text{O}_5^+ + 2\text{H}_2\text{O} \rightarrow \text{C}_6\text{H}_{12}\text{O}_6 + \text{H}_3\text{O}^+$.

Table 3. Average Bond Lengths and Corresponding Standard Deviations (in Å) of Selected Configurations along the Reaction Pathway $\text{C}_6\text{H}_{11}\text{O}_5^+ + 2\text{H}_2\text{O} \rightarrow \text{C}_6\text{H}_{12}\text{O}_6 + \text{H}_3\text{O}^+$

	C1–O _W	H _W –O _W	C1–O _S
PI4	2.49 ± 0.18	1.00 ± 0.02	1.28 ± 0.02
TS10	2.00 ± 0.04	1.03 ± 0.03	1.34 ± 0.04
PI5	1.56 ± 0.03	1.08 ± 0.04	1.40 ± 0.05
PI6	1.44 ± 0.05	2.03 ± 0.35	1.46 ± 0.05

^a Atom nomenclature is presented in Figure 1.

diffusion of the proton from the solvent to the neighborhood of the glycosidic oxygen. The reactant intermediate R6 is connected with PI3 via the saddle point TS9, which is at CV1 = 0.28 and CV2 = 0.42. The transition state TS9 is 25.0 kcal mol⁻¹ above R1. The process from R6 to PI3 corresponds to the proton transfer to the glycosidic oxygen O1, and a further separation between glucose and oxacarbenium species.

3.2. Regeneration of Proton Species. As discussed above, the configuration of PI3 clearly indicates that the formation of an α -glucose and regeneration of acid proton (as shown in Step 2) would occur via hydration of the oxacarbenium ion. Therefore, we selected PI3 as the initial configuration in a second metadynamics computation to simulate the reaction of Step 2. The free energy surface as a function of the CVs (CV3 and CV4) is presented in Figure 5 and snapshots along the reaction coordinate (with selected water molecules only) are presented in Figure 6. Snapshots of each configuration including all water molecules are presented in Figure SI3 of the Supporting Information. The average lengths and corresponding standard deviations of selected bonds at the bottom of the various energy basins are presented in Table 3. The standard deviations -

are computed from all the configurations falling into the region where the free energy is within ~1.5 kcal mol⁻¹ of each minimum.

The lowest energy of the reactant basin in Figure 5 is centered at CV3 = 0.09 and CV4 = 0.91, corresponding to state PI4. The nomenclatures PI3 and PI4 are used to distinguish the same intermediate state along the hydrolysis reaction in two respective simulations that correspond to different CVs. By manually converting the average bond lengths of C1–O_W and H_W–O_W of PI3 into CV3 and CV4, the energy of PI3 can be located at the free energy surface generated from the second metadynamics simulation, as shown in Figure 5. The energy of PI3 is observed to be 0.9 kcal mol⁻¹ less stable than that of PI4, and the bond length of C1–O_W is 2.49 Å for PI4, 0.21 Å shorter than the value at PI3. These differences are attributable to the different heights of Gaussian bias functions and CVs selected in the two calculations. The smaller average height of Gaussian hills and more targeted CVs provide a more detailed sampling of this intermediate state in the second simulation, but the close agreement between the energy and geometrical parameters of PI3 and PI4 indicates a good consistency and energy convergence of the two separate simulations.

The reaction continues as the bond length of C1–O_W decreases, passing through a saddle point TS10 and reaching a product basin PI5 at CV3 = 0.82 and CV4 = 0.89. This energy is 1.0 kcal mol⁻¹ above the free energy of PI4. The distance between C1 and O_W in TS10 is 2.00 Å, consistent with the value obtained from the acid-catalyzed dehydration of fructofuranose.¹³ Inspection of PI5 in Figure 6 shows clearly that a protonated α -glucose is generated. The bond length of C1–O_W decreases from 2.49 Å in PI4 to 1.56 Å at PI5. The configuration of the protonated α -glucose ring at PI5 has changed back to the most stable ${}^4\text{C}_1$ conformation.

The protonated α -glucose is not thermodynamically stable, as the proton diffuses almost without barrier to the solvent medium, leading to the final product basin PI6 where one β -glucose, one α -glucose molecule, and an acid proton are identified. PI6 is located at CV3 = 0.87 and CV4 = 0.03, which is 7.0 kcal mol⁻¹ more stable than PI5. Inspection of PI6 snapshot shows that the proton forms a H_3O_2^+ species, and the bond length H_W–O_W is 2.03 Å. The average C1–O_W bond length in α -glucose is 1.44 Å with a standard deviation of 0.05 Å, consistent with reported equilibrium geometrical value of monohydrated α -glucose using FT-Raman spectrum⁵⁷ and the value of α -glucose in aqueous solution from molecular dynamics simulation.²⁰ The snapshot of PI6 in Figure 6 indicates that the proton is connected to the –OH groups on C1 and C2 in α -glucose via three hydrogen bonds, and a direct interaction between two glucose molecules is minimized in the periodic supercell.

The CB hydrolysis reaction free energy calculated from reactants and products at infinite separation in aqueous phase, $\Delta G_{\text{aq},\text{IM}}^{\text{inf}}(298\text{ K})$, was determined by static quantum chemical calculations using reaction Rxn-1. First, the computed gas phase reaction free energy $\Delta G_{\text{gas},\text{IM}}^{\text{inf}}(298\text{ K})$ is -4.7 kcal mol⁻¹. The calculated solvation free energies ($\Delta_s G$) of α -glucose, β -glucose, and CB are -20.4, -21.8, and -34.7 kcal mol⁻¹, respectively. Using the experimental value of $\Delta_s G$ of H_2O (-6.3 kcal mol⁻¹),⁵⁸ the computed aqueous phase infinite reaction free energy $\Delta G_{\text{aq},\text{IM}}^{\text{inf}}(298\text{ K})$ is -5.9 kcal mol⁻¹, which is consistent with the reported value of ≤ -3.0 kcal mol⁻¹ obtained from enzyme catalytic CB hydrolysis experiments,⁴ and -3.8 kcal mol⁻¹ computed from a thermodynamic pathway using relevant

experimental data.⁵



On the other hand, to evaluate the energy required to bring solvated, protonated CB to infinite separation, we have estimated from static electronic structure calculations the $\Delta G_{\text{aq},1\text{M}}^{\text{inf}}$ (298 K) of reaction Rxn-2



where, CB corresponds to CB in the *syn*-conformation, and n corresponds to the number of explicit water molecules in order to balance Rxn-2. R3' corresponds to protonated CB, which was extracted from configuration R3 (Figure 3) by deleting redundant solvation water molecules. Two R3' models were used, $\text{CB}\cdot(\text{H}_{15}\text{O}_7^+)$ or $\text{CB}\cdot(\text{H}_{13}\text{O}_6^+)$, which contains 7 and 6 water molecules to maintain the local configuration between proton and CB. $\text{CB}\cdot(\text{H}_{15}\text{O}_7^+)$ or $\text{CB}\cdot(\text{H}_{13}\text{O}_6^+)$ were subject to static electronic structure optimizations. The optimized configurations of these two clusters are presented in Figure 7, together with selected geometrical parameters. The Cartesian coordinates of the clusters are provided in the Supporting Information. Two R3' models were used

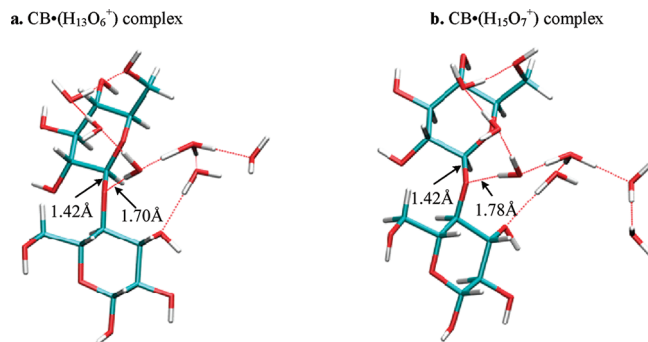


Figure 7. Optimized geometries of $\text{CB}\cdot(\text{H}_{13}\text{O}_6^+)$ and $\text{CB}\cdot(\text{H}_{15}\text{O}_7^+)$ in gas phase, calculated at the B3LYP/6-31G(d,p) level.

in order to check the convergence of $\Delta G_{\text{aq},1\text{M}}^{\text{inf}}$ (298 K) with the number of added water molecules. The $\Delta_s G$ of $\text{CB}\cdot(\text{H}_{15}\text{O}_7^+)$ and $\text{CB}\cdot(\text{H}_{13}\text{O}_6^+)$ using the continuum solvation model SMD⁵² were computed to be $-88.2 \text{ kcal mol}^{-1}$ and $-85.7 \text{ kcal mol}^{-1}$. Using the experimental values of $\Delta_s G$ of H_2O ($-6.3 \text{ kcal mol}^{-1}$)⁵⁸ and H_3O^+ ($-110.2 \text{ kcal mol}^{-1}$),⁵⁹ we computed the aqueous phase reaction Gibbs free energy of (Rxn-2) to be 22.2 and 22.0 kcal mol^{-1} in the case where R3' is $\text{CB}\cdot(\text{H}_{15}\text{O}_7^+)$ and $\text{CB}\cdot(\text{H}_{13}\text{O}_6^+)$ respectively. Since the energy difference from our metadynamics calculation between R1 and R3 is 5.5 kcal mol^{-1} , the free energy of bringing the reactants from infinite separation to R1 is deduced to be $(22.2 - 5.5) = 16.7 \text{ kcal mol}^{-1}$.

Figure 8 summarizes the free energy pathways of acid-catalyzed CB hydrolysis, which includes the energy required to bring R1 and PI6 to an infinite separation. The lowest energy barrier is 32.5 kcal mol^{-1} , corresponding to the stepwise RP1 hydrolysis mechanism. Although uncertainties due to the use of exchange-correlation functionals in computations of heats of reaction and energy barriers are of the order of 2–5 kcal mol^{-1} ,^{61–64} the calculated energy barrier is consistent with experimental activation energies of acid-catalyzed CB hydrolysis.^{1,2}

A second competitive reaction path is observed to be 1.8 kcal mol^{-1} more activated than RP1, corresponding to the concerted RP2 hydrolysis mechanism, along which the protonation and dissociation of the glycosidic bond occur simultaneously. In order to determine whether a difference of 1.8 kcal mol^{-1} between the two reaction paths is larger than the statistical error of our metadynamics sampling, we have evaluated the accuracy of the reconstructed free energy surfaces according to eq E.4 proposed by Bussi et al:⁶⁰

$$\langle \varepsilon^2 \rangle = \frac{S^2 w}{\beta D \tau_g} \left(\frac{\delta_s \sqrt{2\pi}}{S} \right)^d \sum_{k \neq 0} \frac{\exp\left(-\frac{\pi^2 k^2 \delta_s^2}{2S^2}\right)}{\pi^2 k^2} \quad (\text{E.4})$$

In this equation, S is the size of the free energy well, w is the Gaussian hill height, δ_s is the hill width, τ_g is the metadynamics

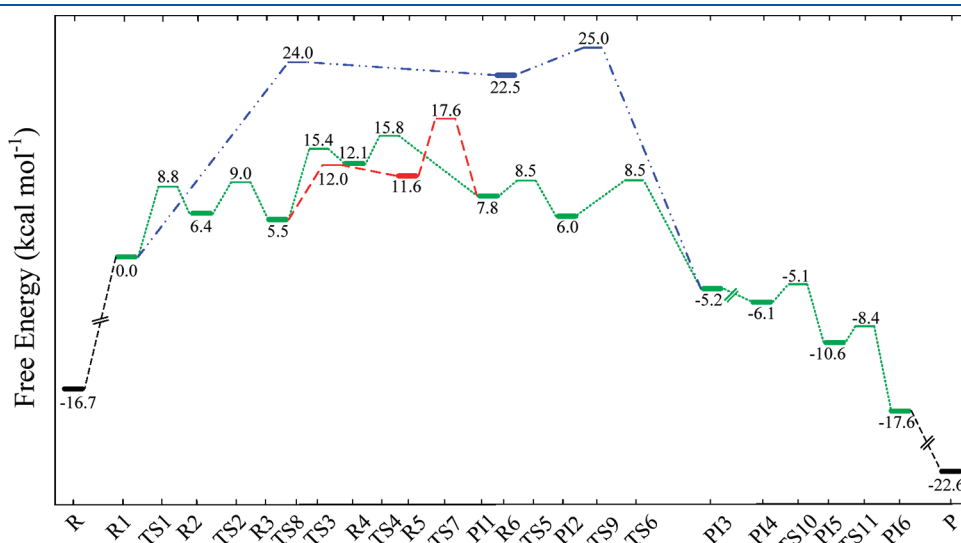


Figure 8. Energy profile at 300 K of acid-catalyzed hydrolysis of *syn*-CB. The nomenclature in the *x*-axis corresponds to those used in Figures 2–6. R and P correspond to the reactants and products at infinite separation. Broken lines (-//-) are used to connect two energy minima for which no TS is provided. The green dotted line, red dashed line, and blue dash-dotted lines correspond to RP1 ($\text{R1} \rightarrow \text{TS4} \rightarrow \text{P13}$), RP2 ($\text{R1} \rightarrow \text{TS7} \rightarrow \text{P13}$), and RP3 ($\text{R1} \rightarrow \text{TS9} \rightarrow \text{P13}$), respectively.

time step, D is the diffusion coefficient of the CV, which can be calculated from the integration of the velocity autocorrelation function, d is the dimensionality of the CV space, k is a d dimensional vector with positive integers, and β is equal to $(k_B T)^{-1}$, in which k_B is the Boltzmann constant and T is the temperature. The smallest diffusion coefficient in each metadynamics calculation is used to determine the corresponding $\langle \varepsilon^2 \rangle$. The calculated statistical errors of the metadynamics simulations of Step 1 and Step 2 are 1.8 and 0.8 kcal mol⁻¹, respectively. Clearly in this simulation, we are unable to favor reaction path RP1 over RP2 because the difference between the energy barriers lies within $\langle \varepsilon^2 \rangle$.

The energy demand for transferring a proton species from infinity to a point near the glycosidic bond accounts for the bulk of the energy required to break the glycosidic bond. This observation is consistent with the study of acid-catalyzed hydrolysis of xylobiose,¹¹ which showed that the diffusion of a proton from infinity to the neighborhood of xylobiose is 10–15 kcal mol⁻¹ endothermic, while the subsequent formation of the oxacarbenium ion is \sim 10 kcal mol⁻¹ activated.

Several computational works have recently been conducted on acid-catalyzed dehydration of monosaccharides that include β -xylose,¹¹ β -glucose,¹² and α -fructose.¹³ Here, we compare our computed results with Qian's work of β -glucose dehydration,¹² considering the similar chemical structures of monosaccharides (α -glucose vs β -glucose) and the comparable computational levels of these two studies. Qian and co-workers performed CPMD-metadynamics simulations of the acid-catalyzed dehydration of β -glucose.¹² The reaction steps, studied in a cubic supercell (14.4³ Å³) with 76 solvent molecules, correspond to our steps connecting P to PI4. In general, we find our energy barriers (for α -glucose) to be lower than those reported by Qian et al.:¹² for the step P \rightarrow TS11 (protonation), we obtained 14.2 versus 20–25 kcal mol⁻¹; for PI5 \rightarrow TS10 (dehydration), we obtained 5.5 versus \sim 10 kcal mol⁻¹; and for the overall endothermicity of P \rightarrow PI4 (formation of the oxacarbenium), we obtained 16.5 versus \sim 5 kcal mol⁻¹. The energy differences between these two studies are attributable to the well-known kinetic anomeric effect,^{65–68} and to the fact that our cells contain two solute molecules.

4. CONCLUSION

Metadynamics simulations were carried out to determine the reaction pathways and free energy surface for the acid-catalyzed hydrolysis of *syn*-CB in aqueous phase. Two low-energy reaction pathways are identified for the formation of glucose and oxacarbenium ion. One corresponds to a stepwise reaction mechanism that proceeds via formation of a protonated CB, followed by dissociation of the glycosidic bond. The other corresponds to a concerted mechanism in which protonation and dissociation occur simultaneously.

The computated activation free energies of the stepwise and concerted reaction steps are 32.5 and 34.3 kcal mol⁻¹, which in either case is consistent with reported experimental activation energies of CB hydrolysis under dilute acid conditions. The difference between the two energy barriers is within the statistical error of our metadynamics sampling (\pm 1.8 kcal mol⁻¹). The transport of proton from the bulk water to the vicinity of the glycosidic oxygen corresponds to the bulk of the free energy barrier, mainly because of the high affinity of proton to water molecules.

The conformation of the nonreducing ring is observed to undergo a significant modification before the rupture of the glycosidic bond, changing from a ⁴C₁ to an E₃ form in the stepwise pathway and to an ⁴E form in the concerted pathway. Once the dissociation of the glycosidic bond takes place, the nonreducing ring is transformed to an oxacarbenium ion in the ⁴H₃ half-chair conformation.

Hydration of the oxacarbenium ion followed by regeneration of acid proton to finally produce one α -glucose and one β -glucose is nearly barrierless. The computed reaction Gibbs free energy of CB hydrolysis is -5.9 kcal mol⁻¹, consistent with the reported experimental data.

■ ASSOCIATED CONTENT

S Supporting Information. The Supporting Information contains the configurations of the selected snapshots that are collected from metadynamics simulations. In addition, it includes the configuration and Cartesian coordinates of the CB \cdot (H₁₅O₇⁺) and CB \cdot (H₁₃O₆⁺) clusters used in the static electronic structure calculations. This material is available free of charge via the Internet at <http://pubs.acs.org>.

■ AUTHOR INFORMATION

Corresponding Author

*E-mail: alejandro.montoya@sydney.edu.au.

■ ACKNOWLEDGMENT

This work has been funded by the Australian Research Council through Discovery Grant DP1096802. The authors acknowledge the Australian National Computational Infrastructure (NCI) for the computational time allocated to this project.

■ REFERENCES

- (1) Dadach, Z. E.; Kaliaguine, S. *Can. J. Chem. Eng.* **1993**, *71*, 880.
- (2) Pinto, J. H. Q.; Kaliaguine, S. *AIChE J.* **1991**, *37*, 905.
- (3) Pilath, H. M.; Nimlos, M. R.; Mittal, A.; Himmel, M. E.; Johnson, D. K. *J. Agric. Food. Chem.* **2010**, *58*, 6131.
- (4) Tewari, Y. B.; Goldberg, R. N. *J. Biol. Chem.* **1989**, *264*, 3966.
- (5) Tewari, Y. B.; Lang, B. E.; Decker, S. R.; Goldberg, R. N. *J. Chem. Thermodyn.* **2008**, *40*, 1517.
- (6) Moiseiw, Y. V.; Khalturinskii, N. A.; Zaikov, G. E. *Carbohydr. Res.* **1976**, *51*, 23.
- (7) Belkacemi, K.; Abatzoglou, N.; Overend, R. P.; Chornet, E. *Ind. Eng. Chem. Res.* **1991**, *30*, 2416.
- (8) Jencks, W. P. *Chem. Soc. Rev.* **1981**, *10*, 345.
- (9) BeMiller, J. N. Acid-Catalyzed Hydrolysis of Glycosides. In *Advances in Carbohydrate Research*; Wolfrom, M. L., Ed.; Academic Press Inc.: New York, 1967; Vol. 22, p 25.
- (10) Stubbs, J. M.; Marx, D. *Chem.—Eur. J.* **2005**, *11*, 2651.
- (11) Dong, H.; Nimlos, M. R.; Himmel, M. E.; Johnson, D. K.; Qian, X. *J. Phys. Chem. A* **2009**, *113*, 8577.
- (12) Liu, D.; Nimlos, M. R.; Johnson, D. K.; Himmel, M. E.; Qian, X. *J. Phys. Chem. A* **2010**, *114*, 12936.
- (13) Caratzoulas, S.; Vlachos, D. G. *Carbohydr. Res.* **2011**, *346*, 664.
- (14) Strati, G. L.; Willett, J. L.; Momany, F. A. *Carbohydr. Res.* **2002**, *337*, 1833.
- (15) Bosma, W. B.; Appell, M.; Willett, J. L.; Momany, F. A. *J. Mol. Struct. (THEOCHEM)* **2006**, *776*, 21.
- (16) Appell, M.; Strati, G.; Willett, J. L.; Momany, F. A. *Carbohydr. Res.* **2004**, *339*, 537.

- (17) Barrows, S. E.; Dulles, F. J.; Cramer, C. J.; French, A. D.; Truhlar, D. G. *Carbohydr. Res.* **1995**, *276*, 219.
- (18) Barrows, S. E.; Storer, J. W.; Cramer, C. J.; French, A. D.; Truhlar, D. G. *J. Comput. Chem.* **1998**, *19*, 1111.
- (19) Ma, B.; Schaefer, H. F., III; Allinger, N. L. *J. Am. Chem. Soc.* **1998**, *120*, 3411.
- (20) Corchado, J. C.; Sanchez, M. L.; Aguilar, M. A. *J. Am. Chem. Soc.* **2004**, *126*, 7311.
- (21) Cocinero, E. J.; Gamblin, D. P.; Davis, B. G.; Simons, J. P. *J. Am. Chem. Soc.* **2009**, *131*, 11117.
- (22) Sugiyama, J.; Vuong, R.; Chanzy, H. *Macromolecules* **1991**, *24*, 4168.
- (23) Atalla, R. H.; VanderHart, D. L. *Solid State Nucl. Magn. Reson.* **1999**, *15*, 1.
- (24) Nishiyama, Y.; Langan, P.; Chanzy, H. *J. Am. Chem. Soc.* **2002**, *124*, 9074.
- (25) Brown, C. J. *J. Chem. Soc. A* **1966**, 927.
- (26) Chu, S. S. C.; Jeffrey, G. A. *Acta Crystallogr., Sect. B* **1968**, *24*, 830.
- (27) Cheetham, N. W. H.; Dasgupta, P.; Ball, G. E. *Carbohydr. Res.* **2003**, *338*, 955.
- (28) Pereira, C. S.; Kony, D.; Baron, R.; Muller, M.; van Gunsteren, W. F.; Hunenberger, P. H. *Biophys. J.* **2006**, *90*, 4337.
- (29) Larsson, E. A.; Staaf, M.; Soederman, P.; Hoeoeg, C.; Widmalm, G. *J. Phys. Chem. A* **2004**, *108*, 3932.
- (30) Laio, A.; VandeVondele, J.; Rothlisberger, U. *J. Chem. Phys.* **2002**, *116*, 6941.
- (31) Laio, A.; Gervasio, F. L. *Rep. Prog. Phys.* **2008**, *71*, 126601/1.
- (32) Park, J. M.; Laio, A.; Iannuzzi, M.; Parrinello, M. *J. Am. Chem. Soc.* **2006**, *128*, 11318.
- (33) Cucinotta, C. S.; Ruini, A.; Catellani, A.; Stirling, A. *ChemPhysChem* **2006**, *7*, 1229.
- (34) Schreiner, E.; Nair, N. N.; Marx, D. *J. Am. Chem. Soc.* **2008**, *130*, 2768.
- (35) Car, R.; Parrinello, M. *Phys. Rev. Lett.* **1985**, *55*, 2471.
- (36) Goedecker, S.; Teter, M.; Hutter, J. *Phys. Rev. B: Condens. Matter* **1996**, *54*, 1703.
- (37) Becke, A. D. *Phys. Rev. A: Gen. Phys.* **1988**, *38*, 3098.
- (38) Lee, C.; Yang, W.; Parr, R. G. *Phys. Rev. B: Condens. Matter* **1988**, *37*, 785.
- (39) Nose, S. *J. Chem. Phys.* **1984**, *81*, 511.
- (40) Zahn, D. *J. Phys. Chem. B* **2003**, *107*, 12303.
- (41) Frisch, M. J.; Trucks, G. W.; Schlegel, H. B.; Scuseria, G. E.; Robb, M. A.; Cheeseman, J. R.; Scalmani, G.; Barone, V.; Mennucci, B.; Petersson, G. A.; Nakatsuji, H.; Caricato, M.; Li, X.; Hratchian, H. P.; Izmaylov, A. F.; Bloino, J.; Zheng, G.; Sonnenberg, J. L.; Hada, M.; Ehara, M.; Toyota, K.; Fukuda, R.; Hasegawa, J.; Ishida, M.; Nakajima, T.; Honda, Y.; Kitao, O.; Nakai, H.; Vreven, T.; Montgomery, J. A., Jr.; Peralta, J. E.; Ogliaro, F.; Bearpark, M.; Heyd, J. J.; Brothers, E.; Kudin, K. N.; Staroverov, V. N.; Kobayashi, R.; Normand, J.; Raghavachari, K.; Rendell, A.; Burant, J. C.; Iyengar, S. S.; Tomasi, J.; Cossi, M.; Rega, N.; Millam, J. M.; Klene, M.; Knox, J. E.; Cross, J. B.; Bakken, V.; Adamo, C.; Jaramillo, J.; Gomperts, R.; Stratmann, R. E.; Yazyev, O.; Austin, A. J.; Cammi, R.; Pomelli, C.; Ochterski, J. W.; Martin, R. L.; Morokuma, K.; Zakrzewski, V. G.; Voth, G. A.; Salvador, P.; Dannenberg, J. J.; Dapprich, S.; Daniels, A. D.; Farkas, Ö.; Foresman, J. B.; Ortiz, J. V.; Cioslowski, J.; Fox, D. J. *Gaussian 09*, revision A.1; Gaussian, Inc.: Wallingford, CT, 2009.
- (42) Coutinho, K.; Canuto, S. *DICE*, version 2.9; University of São Paulo: São Paulo, Brazil, 2003.
- (43) Ensing, B.; De Vivo, M.; Liu, Z.; Moore, P.; Klein, M. L. *Acc. Chem. Res.* **2006**, *39*, 73.
- (44) Iannuzzi, M.; Laio, A.; Parrinello, M. *Phys. Rev. Lett.* **2003**, *90*, 238302/1.
- (45) Gunaydin, H.; Houk, K. N. *J. Am. Chem. Soc.* **2008**, *130*, 15232.
- (46) Petersen, L.; Ardevol, A.; Rovira, C.; Reilly, P. *J. Phys. Chem. B* **2009**, *113*, 7331.
- (47) Barker, I. J.; Petersen, L.; Reilly, P. *J. Phys. Chem. B* **2010**, *114*, 15389.
- (48) Humphrey, W.; Dalke, A.; Schulten, K. *J. Mol. Graphics* **1996**, *14*, 33.
- (49) Csonka, G. I. *J. Mol. Struct. (THEOCHEM)* **2002**, *584*, 1.
- (50) Hayik, S.; Bhat, K. L.; Bock, C. W. *Struct. Chem.* **2004**, *15*, 133.
- (51) Miura, N.; Taniguchi, T.; Monde, K.; Nishimura, S.-I. *Chem. Phys. Lett.* **2006**, *419*, 326.
- (52) Marenich, A. V.; Cramer, C. J.; Truhlar, D. G. *J. Phys. Chem. B* **2009**, *113*, 6378.
- (53) Cramer, C. J. *Essentials of Computational Chemistry: Theories and Models*; John Wiley & Sons Ltd: New York, 2004.
- (54) Whitfield, D. M. *Adv. Carbohydr. Chem. Biochem.* **2009**, *62*, 83.
- (55) Sinnott, M. L. *Chem. Rev.* **1990**, *90*, 1171.
- (56) Andrews, C. W.; Fraser-Reid, B.; Bowen, J. P. *ACS Symp. Ser.* **1993**, *539*, 114.
- (57) Corbett, E. C.; Zichy, V.; Goral, J.; Passingham, C. *Spectrochim. Acta, Part A* **1991**, *47A*, 1399.
- (58) Cramer, C. J.; Truhlar, D. G. *J. Comput.-Aided Mol. Des.* **1992**, *6*, 629.
- (59) Pliego, J. R., Jr.; Riveros, J. M. *Phys. Chem. Chem. Phys.* **2002**, *4*, 1622.
- (60) Bussi, G.; Laio, A.; Parrinello, M. *Phys. Rev. Lett.* **2006**, *96*, 090601/1.
- (61) Cascella, M.; Raugei, S.; Carloni, P. *J. Phys. Chem. B* **2004**, *108*, 369.
- (62) Pan, B.; Ricci, M. S.; Trout, B. L. *J. Phys. Chem. B* **2011**, *115*, 5958.
- (63) Blumberger, J.; Ensing, B.; Klein, M. L. *Angew. Chem., Int. Ed.* **2006**, *45*, 2893.
- (64) Hehre, W. J. *A Guide to Molecular Mechanics and Quantum Chemical Calculations*; Wavefunction, Inc., 2003.
- (65) Cieplak, A. S. *J. Am. Chem. Soc.* **1981**, *103*, 4540.
- (66) Thatcher, G. R. *J. ACS Symp. Ser.* **1993**, *539*, 6.
- (67) Juaristi, E.; Cuevas, G. *The Anomeric Effect*; CRC Press: Boca Raton, FL, 1995.
- (68) Deslongchamps, P. *Stereoelectronic Effects in Organic Chemistry*; Pergamon: New York, 1983; p 209.